Journal of Molecular Graphics and Modelling 44 (2013) 168–176

Contents lists available at ScienceDirect

Journal of Molecular Graphics and Modelling

journal homepage: www.elsevier.com/locate/JMGM

# Modeling of multifunctional donor-bridge-acceptor 4,6-di(thiophen-2-yl)pyrimidine derivatives: A first principles study

Ahmad Irfan[a,*], Abdullah G. Al-Sehemi[a,b], Mohammad Sultan Al-Assiri[c,d]

[a] Department of Chemistry, Faculty of Science, King Khalid University, Abha 61413, P.O. Box 9004, Saudi Arabia
[b] Unit of Science and Technology, Faculty of Science, King Khalid University, Abha 61413, P.O. Box 9004, Saudi Arabia
[c] Department of Physics, Faculty of Sciences and Arts, Najran University, P.O. Box 1988, Najran 11001, Saudi Arabia
[d] Promising Centre for Sensors and Electronic Devices (PCSED), Najran University, P.O. Box 1988, Najran 11001, Saudi Arabia

ARTICLE INFO

*Article history:*
Accepted 3 June 2013
Available online 19 June 2013

*Keywords:*
Density functional theory
Time dependent density functional theory
Electronic properties
Reorganization energy
Charge transfer

ABSTRACT

We have modeled multifunctional compounds by pi-elongation and push–pull strategy from the 4,6-di(thiophen-2-yl)pyrimidine. The ground state geometries have been optimized by density functional theory while excited state geometries were optimized by time dependent density functional theory (TDDFT). Structure–property relationship, electronic, optical and charge transfer properties (ionization potential, electron affinity and reorganization energies) were computed and discussed. By TDDFT absorption and emission have been calculated. The computed parameters were compared with available experimental data. The long-range corrected functional (LC-BLYP) is overestimating the highest occupied and lowest unoccupied molecular orbital energies, energy gaps while underestimating the absorption and fluorescence wavelengths. The B3LYP is good to reproduce the experimental data. The intra-molecular charge transfer has been observed from highest occupied molecular orbitals to lowest unoccupied molecular orbitals. The strong electron withdrawing and electron donor groups efficiently reduce the energy gaps. The decrease injection barrier and smaller reorganization energies are revealing that our designed derivatives would be efficient hole as well as electron transfer materials. These derivatives would be good light emitters e.g. blue, green, orange, red and near IR. The predicted values showed that the designed derivatives would be efficient for the organic field effect transistors, photovoltaics and light emitters.



## 1. Introduction

Organic electronics are emergent rapidly in important technological fields [1–4]. Conjugated materials are being used in batteries [5–9], electroluminescent devices [10], field-effect transistors [11], and photovoltaics [12], etc. The polymers or small molecules are attracting attention due to the low-cost, environment friendly, ease to fabricate and their flexibility than traditional materials, like silicon. Such properties make organic materials ultimate for applications in mobile electronic devices as well. The organic electronic materials have attracted passionate and unremitting interest in recent years. To enhance the charge carrier mobilities and/or the quantum efficiency of organic electronics is under consideration. Oligothiophenes are well-characterized conjugated systems which have been investigated previously [13–16]. These semiconductors are important contenders which have been used in molecular electronics, as light emitting diodes and field-effect transistors [17,18]. The band gap is a way to control the electrical properties, which are strongly governed by the intra-molecular delocalization of π-electrons along the conjugation chain [19]. In optoelectronic devices pi-conjugated oligomers and polymers based on heteropentacenes containing pyrrole, thiophene, and silole have been widely used [20–22]. The OFETs can now compete with other thin film transistors such as amorphous silicon devices [23].

The first organic light-emitting field-effect transistor (OLFET) has been reported in 2003 [24] which is a new class of electro-optical devices. The OLFETs could provide a novel architecture to address open questions concerning charge-carrier recombination and light emission in organic materials [25]. The split-gate LFETs demonstrate a new strategy for ambipolar LFETs to achieve high brightness and efficiency simultaneously [26]. Two active layers of pentacene and *N*,*N*′-ditridecylperylene-3,4,9,10-tetra carboxylic diimide as well as a protecting layer of 2,5-bis(4-biphenyl) thiophene were studied as OLFETs previously [27]. The 4,6-di(thiophen-2-yl)pyrimidine (**1**) has alternate pi-rich and pi-poor units, i.e., thiophene and pyrimidine [28]. We have designed new derivatives of **1** with thiophene, pyrimidine and oligocene units with the aim to enhance optical and charge transfer properties.

Different computational studies are effective tools to design of efficient functional materials (like organic electronic materials),

* Corresponding author. Tel.: +966 72418632; fax: +966 72418426.
*E-mail address:* irfaahmad@gmail.com (A. Irfan).

1093-3263/$ – see front matter © 2013 Elsevier Inc. All rights reserved.
http://dx.doi.org/10.1016/j.jmgm.2013.06.003

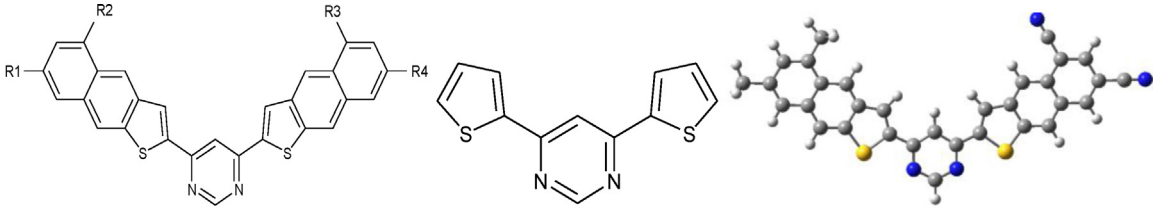


**1** (centre)

**2** = R1, R2 = $CH_3$; R3, R4 = CN

**3** = R1, R2 = $CH_3$; R3, R4 = COOH

**4** = R1, R2 = $CH_3$; R3, R4 = F

**5** = R1, R2 = $CH_3$; R3, R4 = $NO_2$

**6** = R1, R2 = $OCH_3$; R3, R4 = CN

**7** = R1, R2 = $OCH_3$; R3, R4 = COOH

**8** = R1, R2 = $OCH_3$; R3, R4 = F

**9** = R1, R2 = $OCH_3$; R3, R4 = $NO_2$

**10** = R1, R2 = OH; R3, R4 = CN

**11** = R1, R2 = OH; R3, R4 = COOH

**12** = R1, R2 = OH; R3, R4 = F

**13** = R1, R2 = OH; R3, R4 = $NO_2$

**Fig. 1.** The optimized structures of **1** (center) and its derivatives investigated in the presented study (the structure at right is an example of derivative, i.e., **2**).

to predict their properties and to explain the available experimental data. New derivatives have been designed by push–pull strategy and elongating the bridge with the aim to reduce the HOMO–LUMO energy gap, improved intra-molecular charge transfer which would tailor the electronic, optical and charge transfer properties, see Fig. 1. The effect of electron activating groups, deactivating groups and bridge has been studied on the geometries, dipole moments, electronic, spectroscopic (absorption and fluorescence), and charge transfer properties (ionization potentials, electron affinities, reorganization energies) and discussed thoroughly. The structure–property relationship has been discussed. The paper is structured as follows: Section 2 presents an outline of the density functional theory (DFT) and time dependent density functional theory (TDDFT) methodology used, including the rationale for choosing the hybrid functional and the basis set; Section 3 gives the frontier molecular orbitals, electronic, optical and charge transfer properties with detailed comparisons with experimental and theoretical studies; in Section 4 the major conclusions of the present investigation are presented.

## 2. Computational details

The line shape of the lowest gas-phase ultraviolet photoelectron spectroscopy (UPS) band is directly related to the geometry relaxation energy thus to the polaron binding energy [29]. Among the standard DFT [30] functionals, B3LYP provides the best description of the geometry modifications upon ionization [31]. The ground state ($S_0$) geometries have been optimized using density functional theory (DFT). The Becke's three parameter gradient-corrected exchange potential and the Lee–Yang–Parr gradient-corrected correlation potential (B3LYP) [32–34], and 6-31G** basis set [35] has been used for all the calculations. The frequencies have been computed at the same level of theory and no imaginary frequency has been observed. The absorption spectra have been computed by using time dependent density functional theory (TDDFT) which has been proved an efficient approach [36,37]. The excited state ($S_1$) geometries have been optimized at TDDFT [38–44] using B3LYP/6-31G** level of theory. The emission spectra have been computed by using TD-B3LYP [45] and 6-31G** basis set [35].

The efficiency of charge transport within the organic layer(s) plays a key role. The high-charge mobilities favor recombination processes in the bulk where charges can be confined further by means of organic–organic interfaces [46]. The charge transfer rate can be described by Marcus theory via the following equation [47]:

$$W = \frac{V^2}{h(\pi/\lambda k_B T)^{1/2}} \exp\left(-\frac{\lambda}{4k_B T}\right) \quad (1)$$

There are two major parameters that determine self-exchange electron-transfer rates and ultimately charge mobility: (i) the electronic coupling $V$ (transfer integral) between adjacent molecules, which needs to be maximized and (ii) the reorganization energy $\lambda$, which needs to be small for significant transport. The reorganization energy term describes the strength of the electron–phonon (vibration) and can be reliably estimated as twice the relaxation energy of a polaron localized over a single unit.

The reorganization energy is further divided into two parts: $\lambda_{rel}^{(1)}$ and $\lambda_{rel}^{(2)}$, where $\lambda_{rel}^{(1)}$ corresponds to the geometry relaxation energy of one molecule from neutral to charged state, and $\lambda_{rel}^{(2)}$ corresponds to the geometry relaxation energy from charged to neutral state [48]:

$$\lambda = \lambda_{rel}^{(1)} + \lambda_{rel}^{(2)} \quad (2)$$

In the evaluation of $\lambda$, the two terms were computed directly from the adiabatic potential energy surfaces [49,50]:

$$\lambda = \lambda_{rel}^{(1)} + \lambda_{rel}^{(2)} = [E^{(1)}(Y^+) - E^{(0)}(Y^+)] + [E^{(1)}(Y) - E^{(0)}(Y)] \quad (3)$$

Here, $E^{(0)}(Y)$, $E^{(0)}(Y^+)$ are the ground-state energies of the neutral and charged states, $E^{(1)}(Y)$ is the energy of the neutral molecule at the optimized charged geometry and $E^{(1)}(Y^+)$ is the energy of the charged state at the geometry of the optimized neutral molecule. It should be noted that the polarization effects from the surrounding molecules, as well as the charge reorientation, have been neglected to minimize the complications involved in the theoretical calculations [51,52]. The adiabatic ionization potential (IPa) and vertical ionization potential (IPv) have been calculated as:

$$IPa = E^0(Y) + -E^0(Y) \quad \text{and} \quad IPv = E^1(Y)^+ - E^0(Y).$$

The ground state energies of the neutral and cation states represented by $E^0(Y)$ and $E^0(Y)^+$ respectively, and $E^1(Y)^+$ is the energy of cation state at the optimized geometry of the neutral molecule. The adiabatic/vertical electron affinity (EAa)/(EAv) of all molecules has been calculated as under:

$$EAa = E^0(Y) - E^0(Y)^- \quad \text{and} \quad EAv = E^0(Y)^- E^1(Y)^-$$

Here, $E^0(Y)$ corresponds to the ground state energies of the neutral and $E^0(Y)^-$ is the energy of anion states. The term $E^1(Y)^-$ represents the energy of anion state at the optimized geometry of the neutral molecule. All the calculations have been performed by using Gaussian 09 package [53].

Generally, it is esteemed that B3LYP is not to good reproduce the experimental data, i.e., electronic properties and excitation energies, etc. The excitation energies of coumarin-based dyes were reproduced by Stein et al. by using a range-separated hybrid functional [54]. In push–pull oligothiophene biomarkers the absorption and fluorescence wavelengths were studied by long-range-corrected (LC) method [55]. The LC-BLYP has been used to investigate the excited-state properties in a series of coumarin dyes [56]. The range-separation technique is based on a more physical model of the exchange potential. The B3LYP hybrid functional underestimates the vertical excitation energies, especially for larger molecules. It has been already reported that the choice of the range separation parameter is strongly system dependent [57–60]. Moreover, B3LYP/6-31G(d,p) level is adequate which has been applied to computed the different properties and successfully reproduce the experimental data previously [61–65,34,66].

To validate B3LYP for our studied systems, we have also optimized the geometries at ground and excited states by using long-range corrected functional (LC-BLYP). Then we have also computed the absorption and emission wavelengths. Benchmark computational study has been carried out on parent molecule. In first step, we have compared the HOMO energy, LUMO energy and HOMO–LUMO energy gap absorption, and fluorescence of parent molecule with available experimental data at B3LYP/6-31G** and TD-B3LYP/6-31G**//B3LYP/6-31G** level of theories. In next step all above mentioned properties were also computed and compared at TD-LC-BLYP/6-31G**//B3LYP/6-31G** level of theory. Then we have also computed and compared the data at LC-BLYP/6-31G** and TD-LC-BLYP/6-31G**//LC-BLYP/6-31G** level of theory. It can be seen from Sections 3.1 and 3.2 that B3LYP is good choice to reproduce the experimental data.

## 3. Results and discussion

### 3.1. Electronic structure of the ground and first excited states

The distribution patterns of the highest occupied molecular orbitals (HOMOs) and lowest unoccupied molecular orbitals (LUMOs) for the ground states have been shown in Fig. 2. In **1**, the HOMO and LUMO are distributed throughout the backbone. In designed derivatives HOMOs are delocalized toward the electron activating groups, i.e., left side of the systems. In the formation of HOMOs pyrimidine and thiophene rings are also taking part. The LUMOs are localized toward the electron deactivating groups, i.e., pyrimide, thiophene and benzene rings at right side. The HOMOs and LUMOs are also spread over the electron activating as well as electron deactivating groups, respectively. In the formation of HOMOs strong deactivate group has more participation than the LUMO. In ground state comprehensible intra-molecular charge transfer has been observed from donor (push) to acceptor (pull) moieties. Fig. 3 illustrates the distribution patterns of the HOMOs and LUMOs at excited states. The HOMOs are delocalized at the left side while LUMOs are localized toward the right side. The pyrimidine and thiophene rings of the right side are also taking part in the formation of HOMOs. The LUMOs are localized toward the electron deactivating groups, i.e., pyrimide, thiophene and benzene rings at right side. Generally, the HOMOs and LUMOs are distributed on the electron activating and electron deactivating groups. The distribution pattern of the HOMOs and LUMOs at the excited states is alike at the ground states. Moreover, we have noticed that at ground and excited states, the LUMOs are also localized on that moiety which is toward the acceptor group, i.e., strong deactivating group. The thiophene and benzene toward the activating group have no participation in the formation of LUMOs.

The computed HOMO energy, LUMO energy and HOMO–LUMO energy gap of parent molecule (**1**) at ground state by using B3LYP/6-31G** level of theory are −6.19, −1.94 and 4.25 eV, respectively. The calculated HOMO energy, LUMO energy and HOMO–LUMO energy gap are in good agreement with the experimental data, i.e., −5.30, −1.90, and 3.40 eV [28]. While the computed HOMO energy, LUMO energy and HOMO–LUMO energy gap at LC-BLYP/6-31G** level of theory are −9.05, 0.34 and 9.39 eV revealing that LC-BLYP/6-31G** level of theory would be not a good choice for our studied systems. In the next step, we have computed the HOMO energies, LUMO energies and HOMO–LUMO energy gaps of new designed derivatives at the B3LYP/6-31G** level of theory.

The HOMO energies of new designed derivatives are higher while LUMO energies are lower than the parent molecule at both ground and excited states, respectively. The HOMO–LUMO energy gap in new designed systems is smaller than the parent molecule. By introducing the stronger activating groups higher the HOMO energies in the studied derivatives. The trend to higher the HOMO energies on the base of strength of activating group is as $OCH_3 > OH > CH_3$ both at ground and excited states. On other hand, the trend to lower the LUMO energies on the base of strength of activating group is as $OCH_3 < OH < CH_3$ both at ground and excited states. The trend to higher the HOMO energies on the base of

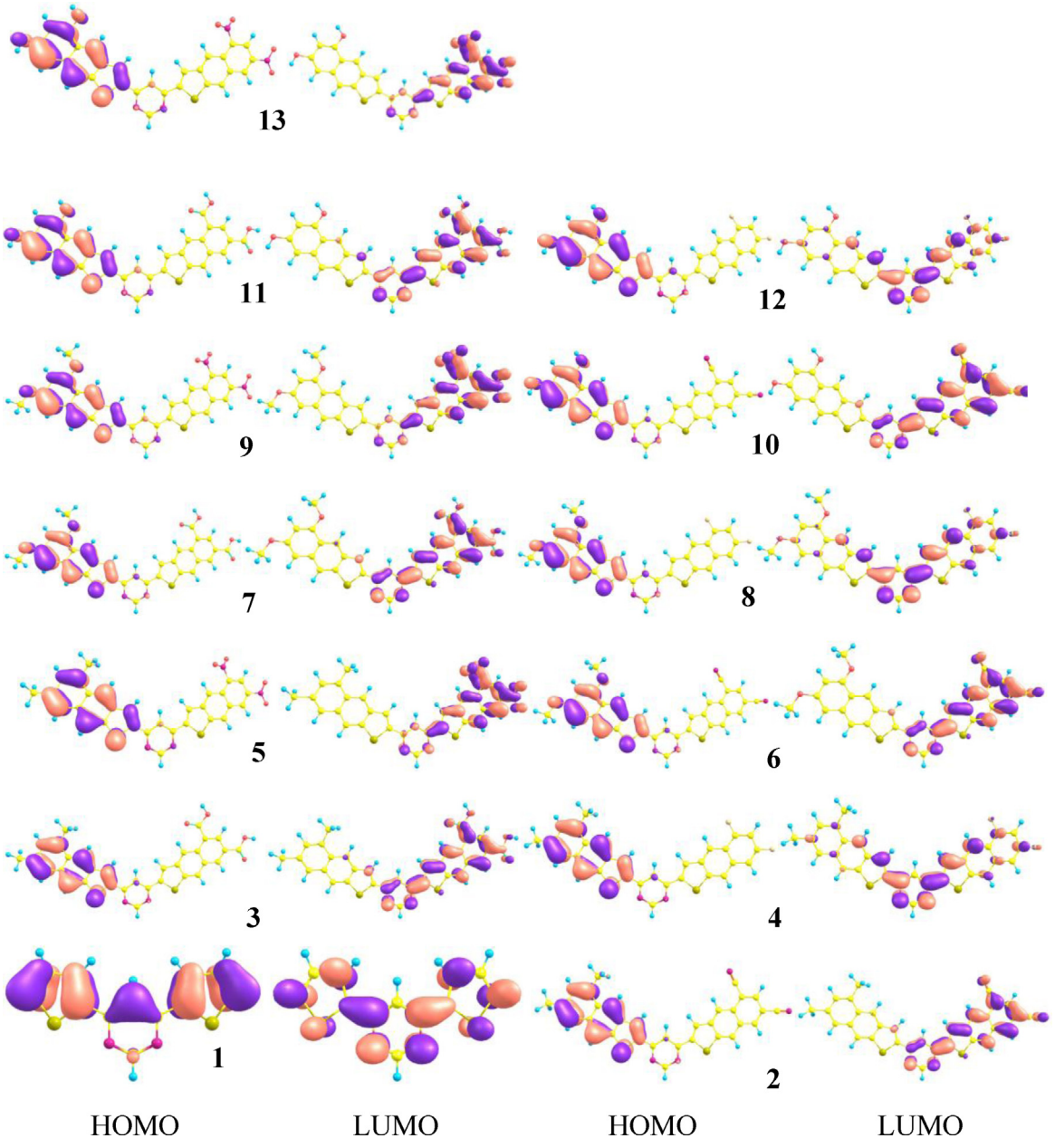


**Fig. 2.** Distribution patterns of the HOMO and LUMO of the ground state.

strength of deactivating group is as F > COOH > CN > $NO_2$ while tendency to lower the LUMO energies is as F > COOH > CN > $NO_2$ both at ground and excited states. The smallest HOMO–LUMO energy gaps have been observed for those systems which have $NO_2$ or CN substituted groups. Such derivatives are effected more which have the strong activating and deactivating groups resulting smaller HOMO–LUMO energy gaps, i.e., **5** (2.26 eV) > **13** (2.12 eV) > **9** (2.06 eV).

In Table 1, we listed the calculated energies for the HOMOs ($E_{HOMO}$), LUMOs ($E_{LUMO}$) and HOMO–LUMO energy gaps ($E_{gap}$) for the **1** and its derivatives at ground and first excited states. We found that the computed $E_{HOMO}$, $E_{LUMO}$ and $E_{gap}$ are in good agreement with the experimental data [28]. The trend of HOMO energies ($E_{HOMO}$) is as follows: **8** > **7** > **12** > **11** > **6** > **9** > **10** > **4** > **13** > **3** > **2** > **5** > **1** while in LUMOs energies ($E_{LUMO}$) is as: **1** > **8** > **12** > **4** > **7** > **11** > **3** > **6** > **10** > **2** > **9** > **13** > **5**. The trend of $E_{gap}$ in studied compounds is **1** > **4** > **12** > **8** > **3** > **11** > **7** > **2** > **10** > **6** > **5** > **13** > **9**, see Table 1. From the trend of HOMO–LUMO energy gaps, we found that stronger activating and deactivating groups reduced the energy gaps more efficiently.

The work function of aluminum is −5.1 eV and the LUMO energy level of **1** is −1.94 eV (see Table 1), the electron injection energy is around 3.16 eV (=−1.94–(−5.1)) from the **1** to Al electrode. Thus it is necessary to lower the LUMO level to improve the electron injection capability. From Table 1, it can be found that LUMO energy levels lowered in new designed derivatives compared to the parent molecule which would lower the injection barrier and improve the electron injection. The electron injection barrier decreases in new designed derivatives as follows: **8** (2.81), **12** (2.78), **4** (2.71), **7** (2.52), **11** (2.50), **3** (2.46), **6** (2.18), **10** (2.16), **2** (2.12), **9** (1.84), **13** (1.83), **5** (1.79). The hole injection energy is around 1.09 eV (=−5.1–(−6.19)) from the **1** to Al electrode. Therefore, to improve the hole injection ability it is necessary to higher the HOMO energy level. The hole injection barrier decreased in all the newly designed derivatives as: **8** (0.08), **7** (0.09), **12** (0.23), **11** (0.24), **6** (0.29), **9** (0.31), **10** (0.35), **4**

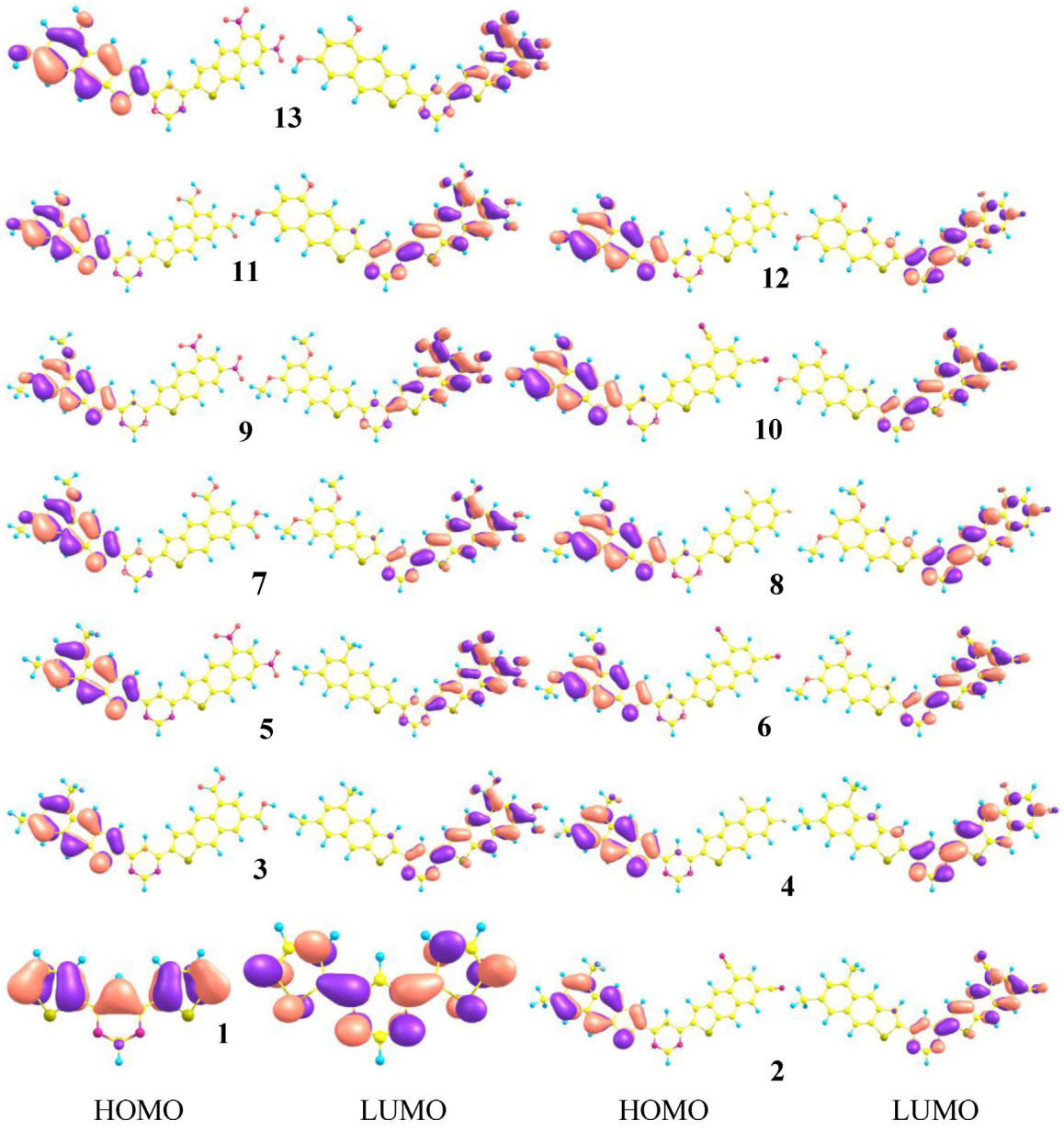


**Fig. 3.** Distribution patterns of the HOMO and LUMO of the first excited state.

**Table 1**
The HOMO energies ($E_{HOMO}$), LUMO energies ($E_{LUMO}$), and HOMO–LUMO energy gaps ($E_{gap}$) in eV for ground and first excited states computed at the B3LYP/6-31G** and TD-B3LYP/6-31G** level of theories, respectively.

| Complexes | Ground state | | | First excited state | | |
|---|---|---|---|---|---|---|
| | $E_{HOMO}$ | $E_{LUMO}$ | $E_g$ | $E_{HOMO}$ | $E_{LUMO}$ | $E_g$ |
| **1** | −6.19 (−5.30) | −1.94 (−1.90) | 4.25 (3.40) | −6.02 | −2.10 | 3.92 |
| **2** | −5.51 | −2.98 | 2.53 | −5.34 | −3.25 | 2.09 |
| **3** | −5.42 | −2.64 | 2.78 | −5.26 | −2.96 | 2.30 |
| **4** | −5.38 | −2.39 | 2.99 | −5.21 | −2.64 | 2.57 |
| **5** | −5.57 | −3.31 | 2.26 | −5.41 | −3.62 | 1.79 |
| **6** | −5.30 | −2.92 | 2.38 | −5.06 | −3.16 | 1.90 |
| **7** | −5.19 | −2.58 | 2.61 | −4.96 | −2.88 | 2.08 |
| **8** | −5.18 | −2.29 | 2.89 | −4.94 | −2.55 | 2.39 |
| **9** | −5.32 | −3.26 | 2.06 | −5.09 | −3.55 | 1.54 |
| **10** | −5.36 | −2.94 | 2.42 | −5.14 | −3.19 | 1.95 |
| **11** | −5.25 | −2.60 | 2.65 | −5.03 | −2.91 | 2.12 |
| **12** | −5.24 | −2.32 | 2.91 | −5.02 | −2.58 | 2.44 |
| **13** | −5.39 | −3.27 | 2.12 | −5.18 | −3.57 | 1.61 |

Values in parentheses are experimental data from Ref. [28].

**Table 2**
The dipole moments (Debye) for **1** and its derivatives of the ground and excited states at the B3LYP/6-31G** level of theory, respectively.

| | | | |
|---|---|---|---|
| **1** | **2** | **3** | **4** |
| 3.55 (3.77) | 6.16 (5.11) | 4.87 (4.22) | 3.89 (3.89) |
| **5** | **6** | **7** | **8** |
| 6.96 (6.37) | 7.91 (7.91) | 5.95 (5.66) | 5.28 (4.87) |
| **9** | **10** | **11** | **12** |
| 8.76 (8.58) | 7.41 (6.58) | 5.20 (5.20) | 4.52 (3.99) |
| **13** | | | |
| 8.27 (7.90) | | | |

The values in parentheses are at excited state.

(0.37), **13** (0.38), **3** (0.41), **2** (0.50), **5** (0.56). The decreased injection barrier for hole and electron revealed that new designed derivatives would be better charge transporter than the parent molecule. The LUMO energies of new designed derivatives are low-lying than the parent molecule revealing that new designed materials would be thermodynamically more stable and charge transport cannot be quenched by losing the electron.

### 3.2. Dipole moment

In Table 2, we have presented the dipole moments ($\mu$) of the ground and first excited states computed at DFT/B3LYP/6-31G** level of theory. Previously we showed that substituted group affects the dipole moment [45]. In this study, we have investigated the effect of electron deactivating groups, electron activating groups and bridge on the dipole moments. By the enhancement of bridge dipole moment generally increases at both ground and excited states compared to parent molecule. Moreover, by substituting the stronger activating and deactivating groups enhance the dipole moment values. We noticed that the effect of weakly activating and deactivating groups on the dipole moment is very little, i.e., **4** and **12** dipole moment is smallest compared to newly designed derivatives.

### 3.3. Photophysical properties

The computed wavelengths (nm) for absorption and fluorescence along *X*-axis and oscillator strengths (*f*) along *Y*-axis have been illustrated in Fig. 4. The main absorption wavelengths of parent molecule at TD-LC-BLYP/6-31G**//B3LYP/6-31G** level of theory are 272 nm ($f$ = 0.8100) and 222 nm ($f$ = 0.1674). Absorption wavelengths of parent molecule at TD-LC-BLYP/6-31G**//LC-BLYP/6-31G** level of theory are 259 nm ($f$ = 0.8019) and 215 nm ($f$ = 0.1720). Fluorescence wavelengths of parent molecule at TD-LC-BLYP/6-31G**//LC-BLYP/6-31G** level of theory are 288 nm ($f$ = 0.8356) and 222 nm ($f$ = 0.1549). The absorption and emission (fluorescence) of parent molecule have also been computed at TD-B3LYP/6-31G**//B3LYP/6-31G** level of theory. Two absorption peaks have been observed at 280 and 327 nm. The computed absorption wavelength 327 nm is in good agreement with the experimental absorption wavelength, i.e., 329 nm [28]. Similarly, two peaks for the computed fluorescence wavelengths have been observed at 292 and 353 nm. The calculated fluorescence wavelength at 353 nm is also in sound agreement with the experimental data, i.e., 378 nm [28]. These results are revealing that our adopted methodology is reasonable and accurate choice while LC-BLYP is underestimating the absorption and fluorescence wavelengths for parent molecule. Thus we have computed the absorption and emission spectra for new designed derivatives at the TD-B3LYP/6-31G**//B3LYP/6-31G** level of theory.

The **2** showed absorption peaks at 349, 427, and 554 nm. By introducing the COOH (**3**) in place of CN showed prominent absorption wavelengths peaks at 352, 438 and 502 nm. The F substitution

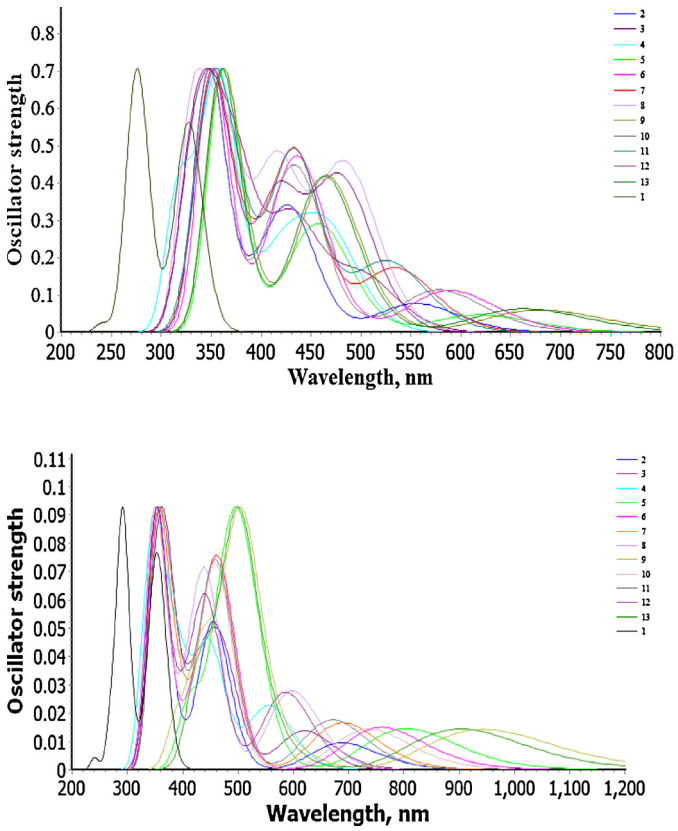


**Fig. 4.** The absorption (top) and fluorescence (bottom) spectra computed at TD-B3LYP/6-31G** level of theory. Note: The experimental absorption wavelengths ($\lambda_a$) = 329 nm; emission wavelength fluorescence ($\lambda_e$) = 378 nm from Ref. [28].

(**4**) in place of CN showed the peaks at 359 and 469 nm. The **5** showed peaks at 364, 467 and 619 nm. By substituting the CN and nitro groups the absorption wavelength are being red shifted. The following prominent absorption peaks have been observed for **6** (350, 447 and 588 nm), **7** (354, 438 and 534 nm), **8** (336, 420 and 485 nm) and **9** (365, 470 and 680 nm). The numerous absorption wavelength peaks have been also observed for **10** (345, 444 and 578 nm), **11** (353, 438 and 527 nm), **12** (358, 421 and 481 nm) and **13** (359, 468 and 664 nm).

The **2** showed fluorescence peaks at 350, 460, and 689 nm. By introducing the COOH (**3**) in place of CN showed peaks at 374, 469 and 620 nm. The F substitution (**4**) in place of CN showed the peaks at 352, 451 and 556 nm. The **5** showed peaks at 505 and 804 nm. The following prominent peaks have been observed for **6** (348, 472 and 759 nm), **7** (351, 468 and 689 nm), **8** (343, 447 and 597 nm) and **9** (508 and 944 nm). The numerous absorption wavelength peaks have been also observed for **10** (346, 466 and 737 nm), **11** (352, 467 and 671 nm), **12** (356, 448 and 586 nm) and **13** (431, 505 and 902 nm). The significant stoke shifts from absorption to fluorescence have been observed in the studied compounds. Multiple emission peaks in whole of the visible region and near IR for some compounds revealed that these would be good emitter materials. The new designed derivatives might be better emitters in the following regions; **2** (blue and red), **3** (blue and orange), **4** (blue and green), **5** (green and near IR), **6** (blue and red), **7** (blue and red), **8** (blue and orange), **9** (green and near IR), **10** (blue and red), **11** (blue and red), **12** (blue and orange) and **13** (green and near IR).

### 3.4. Ionization potential and electron affinity

The ionization potential and electron affinity are good descriptors to shed some light on the charge transfer behavior. The

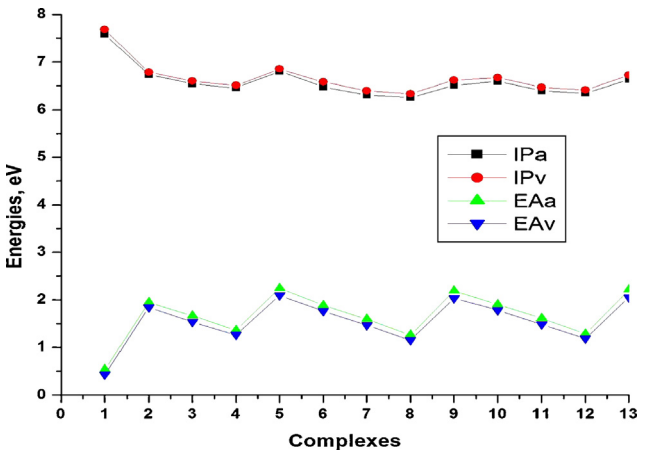


**Fig. 5.** The vertical and adiabatic ionization potentials (IPv/IPa), vertical and adiabatic electronic affinities (EAv/EAa) (in eV) at the B3LYP/6-31G** level of theory.

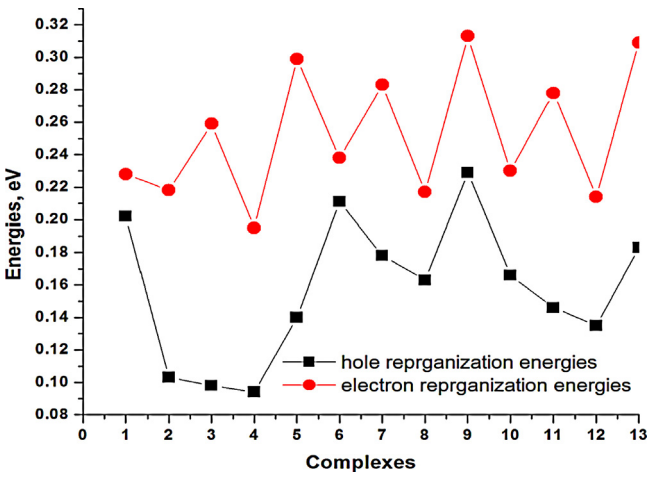


**Fig. 6.** The hole and electron reorganization energies of **1** and its derivatives (in eV) at the B3LYP/6-31G** level of theory.

ionization potential and electron affinity are distinct properties that can be calculated by DFT to estimate the energy barrier for the injection of holes and electrons. The lower ionization potential revealed that material would be better as hole transporter [67] while higher electron affinity leads to be a better electron transport. We have tabulated the adiabatic ionization potential (IPa), vertical ionization potential (IPv), adiabatic electron affinity (EAa), and vertical electron affinity (EAv) in Fig. 5. The IPa/IPv of **2**, **3**, **4** and **5** decreases 0.85/0.90, 1.04/1.08, 1.12/1.17 and 0.78/0.836 eV compared to **1**, respectively. The $OCH_3$ in place of methyl group further lowers the IPa/IPv, i.e., **6**, **7**, **8** and **9** decreases 1.10/1.10, 1.27/1.28, 1.32/1.34 and 1.07/1.06 eV compared to **1**, respectively resulting hole electron injection would increase. The IPa/IPv of **10**, **11**, **12** and **13** also decreases than that of **1**, i.e., 0.99/1.01, 1.18/1.21, 1.23/1.26 and 0.95/0.96 eV, respectively. The hole injection would increase in the sequence $CH_3 < OH < OCH_3$. The EAa/EAv of **2**, **3**, **4** and **5** increases 1.40/1.41, 1.12/1.10, 0.82/0.83 and 1.70/1.66 eV, respectively revealing decreased electron injection barrier compared to the parent molecule. In new designed derivatives less energies are required to create the hole which are smaller than the parent molecule illuminating enhanced hole injection. The EAa/EAv of **6**, **7**, **8** and **9** increases 1.30/1.33, 1.05/1.03, 0.72/0.72 and 1.65/1.60 eV, respectively than that of parent molecule. Moreover, the EAa/EAv of **10**, **11**, **12** and **13** increases 1.36/1.35, 1.07/1.05, 0.74/0.75 and 1.67/1.62 eV, respectively than **1**, see Fig. 5. We found that the electron injection decreases by introducing the stronger electron activating groups in the following tendency: $CH_3 > OH > OCH_3$ while electron injection increases by introducing the stronger electron deactivating groups in the following tendency: $F < COOH < CN < NO_2$. Thus it is expected that the hole as well as electron injection ability of all the new designed derivatives would be improved than **1**.

### 3.5. Reorganization energies

The reorganization energy ($\lambda$) includes the molecular geometry modifications when an electron is added or removed from a molecule (inner reorganization) as well as the modifications in the surrounding medium due to polarization effects (outer reorganization). Here, we focus inner reorganization energy, which reflects the geometric changes in the molecules when going from the neutral to the ionized state and vice versa. It is the sum of two relaxation energy terms [32]: (1) the difference between the energies of the neutral molecule in its equilibrium geometry and in the relaxed geometry characteristic of the ion and (2) the difference between the energies of the radical ion in its equilibrium geometry and in the neutral geometry.

The calculated hole reorganization energy of parent molecule is smaller than the electron one revealing that it might be better hole transfer material. The computed hole reorganization energies of all the new designed derivatives are smaller than the electron reorganization energies indicating these materials might be better hole transfer materials.

The significant effect toward lowering the hole reorganization energy has been observed in **2**–**5**, **7**, **8**, **10**–**13** compared to the parent molecule. Here we have compared the hole reorganization energies of all these materials with already well known materials to shed some light on the charge transfer properties of new designed derivatives. The hole reorganization energies of naphthalene, anthracene, tetracene and pentacene at B3LYP/6-31G** level of theory are 0.186, 0.138, 0.114, 0.098 eV, respectively. The hole reorganization energies of **2**–**5**, **7**, **8**, **10**–**13** are smaller than naphthalene. The hole reorganization energies of **2**–**4** and 12 are smaller than anthracene. The hole reorganization energies of **2**–**4** are smaller than tetracene. The hole reorganization energies of **3** and **4** are smaller than pentacene. It revealed that the new designed materials would be good hole transfer materials and **3** and **4** might be better/comparable to the pentacene which is commonly used hole transfer material. The computed electron reorganization energy of well know and commonly used electron transfer material (mer-Alq3) is 0.276 eV [45]. On the basis of reorganization energy, it seems that the electron mobility of **2**–**4**, **6**, **8**, **10**–**12** derivatives might be better/comparable with *mer*-Alq3. The frontier molecular orbitals (FMOs); highest occupied molecular orbitals (HOMOs) and lowest unoccupied molecular orbitals (LUMOs), ionization potential, electron affinity, reorganization energies suggesting that most of the designed derivatives would be better charge transfer materials, see Fig. 6.

## 4. Conclusions

The B3LYP functional is better than that of LC-BLYP to reproduce the experimental evidences. The comprehensible intra-molecular charge transfer has been observed from highest occupied molecular orbitals to the lowest unoccupied molecular orbitals. The HOMO–LUMO energy gap in new designed systems is smaller than the parent molecule. The stronger activating groups higher the HOMO energies. The trend to augment the HOMO energies on the base of strength of activating group is as $OCH_3 > OH > CH_3$ while contrary effect has been observed to lower the LUMO energies.

The trend to higher the HOMO energies on the base of strength of deactivating group is as F > COOH > CN > $NO_2$ while tendency to lower the LUMO energies is as F > COOH > CN > $NO_2$ both at ground and excited states. The smallest HOMO–LUMO energy gaps have been observed for those systems which have $NO_2$ or CN substituted groups. The stronger activating and deactivating groups reduced the energy gaps more efficiently. The lowered LUMO energy levels are revealing smaller injection barrier resulting improved electron injection in new designed derivatives. The stronger activating and deactivating groups enhance the dipole moment. The nitro-substituents showed fluorescence in visible and toward the longer wavelength, i.e., near IR revealing that these would be efficient sensitizers (dye sensitized solar cell materials). The IPa/IPv of new designed derivatives decreases while EAa/EAv increases compared to **1**. It showed that the injection barrier for hole and electron would decrease. The significant effect toward lowering the hole reorganization energy has been observed in **2–5**, **7**, **8**, **10–13** compared to the parent molecule. The hole reorganization energies of **2–4** and **12** are smaller than anthracene. The hole reorganization energies of **2–4** are smaller than tetracene. The hole reorganization energies of **3** and **4** are smaller than pentacene. The new designed materials would be good hole transfer materials and **3** and **4** might be better/comparable to the pentacene which is commonly used hole transfer material. The electron mobility of **2–4**, **6**, **8**, **10–12** derivatives might be better/comparable with *mer*-Alq3. Finally, it is expected that such type of materials might be better as light emitter field effect transistors. The new designed derivatives would be better light emitters; e.g. blue, green, orange, red and near IR).

## Acknowledgements

Authors would like to acknowledge the support of the Ministry of Higher Education, Kingdom of Saudi Arabia for this research through a grant (PCSED-009-12) under the Promising Centre for Sensors and Electronic Devices (PCSED) at Najran University, Kingdom of Saudi Arabia.

## References

[1] C.D. Dimitrakopoulos, S. Purushothaman, J. Kymissis, A. Callegari, J.M. Shaw, Low-voltage organic transistors on plastic comprising high-dielectric constant gate insulators, Science 283 (1999) 822–824.
[2] H.E. Katz, Recent advances in semiconductor performance and printing processes for organic transistor-based electronics, Chemistry of Materials 16 (2004) 4748–4756.
[3] M. Bendikov, F. Wudl, D.F. Perepichka, Tetrathiafulvalenes, oligoacenenes, and their buckminsterfullerene derivatives: the brick and mortar of organic electronics, Chemical Reviews 104 (2004) 4891–4946.
[4] A. Facchetti, M.H. Yoon, T.J. Marks, Gate dielectrics for organic field-effect transistors: new opportunities for organic electronics, Advanced Materials 17 (2005) 1705–1725.
[5] H.S. Nalwa, Handbook of Organic Conductive Molecules and Polymers, Wiley, New York, 1997.
[6] R.L. Elsenbaumer, T. Skotheim, J.R. Reynolds, Handbook of Conductive Polymers, Dekker, New York, 1998.
[7] K. Mullen, G. Wegner, Electronic Materials: The Oligomers Approach, Wiley-VCH, Weinheim, 1997.
[8] D. Fichou, Handbook of Oligo- and Polythiophenes, Wiley-VCH, Weinheim, 1999.
[9] V.C. Nguyen, K. Potje-Kamloth, Electrical and chemical sensing properties of doped polypyrrole/gold Schottky barrier diodes, Thin Solid Films 338 (1999) 142–148.
[10] R.E. Gill, G.G. Malliaras, J. Wildeman, G. Hadziioannou, Tuning of photo- and electroluminescence in alkylated polythiophenes with well-defined regioregularity, Advanced Materials 6 (1994) 132–135.
[11] F. Garnier, G. Horowitz, X. Peng, D. Fichou, An all-organic "soft" thin film transistor with very high carrier mobility, Advanced Materials 2 (1990) 592–594.
[12] G. Wang, S. Qian, J. Xu, W. Wang, X. Liu, X. Lu, F. Li, Enhanced photovoltaic response of PVK/C60 composite films, Physica B 279 (2000) 116–119.
[13] J. Roncali, Conjugated poly(thiophenes): synthesis, functionalization, and applications, Chemical Reviews 92 (1992) 711–738.
[14] J. Roncali, Synthetic principles for bandgap control in linear pi-conjugated systems, Chemical Reviews 97 (1997) 173–205.
[15] V. Parente, G. Pourtois, R. Lazzaroni, J.L. Bredas, G. Ruani, M. Murgia, R. Zamboni, The vibrational signature of the aluminum/polythiophene interface, Advanced Materials 10 (1994) 319–324.
[16] J.A.E.H. van Haare, M. van Boxtel, R.A.J. Janssen, Pi-dimers of prototype high-spin polaronic oligomers, Chemistry of Materials 10 (1998) 1166–1175.
[17] (a) A. Dobadalapur, L. Torsi, H.E. Katz, Organic transistors: two dimensional transport and improved electrical characteristics, Science 268 (1995) 270–271;
(b) A. Dobadalapur, H.E. Katz, L. Torsi, R.C. Haddon, Organic hetero structure field-effect transistors, Science 269 (1995) 1560–1562;
(c) G. Horowitz, Organic field-effect transistors, Advanced Materials 10 (1998) 365–377;
(d) D. Fichou, Structural order in conjugated oligothiophenes and its implications on opto-electronic devices, Journal of Materials Chemistry 10 (2000) 571–588;
(e) T. Noda, Y. Shirota, 5,5-Bis(dimesitylboryl)-2,2-bithiophene and 5,5-bis(dimesitylboryl)-2,2:5,2-terthiophene as a novel family of electron-transporting amorphous molecular materials, Journal of the American Chemical Society 120 (1998) 9714–9715.
[18] N. Noma, T. Tsuzuki, Y. Shirota, Preparation and electrical conductivities of oligothiophene radical-cation salts, Advanced Materials 7 (1995) 647–652.
[19] J.L. Bredas, Relationship between band gap and bond length alternation in organic conjugated polymers, Chemical Physics 82 (1985) 3808–3811.
[20] J. Zaumseil, H. Sirringhaus, Electron and ambipolar transport in organic field-effect transistors, Chemical Reviews 107 (2007) 1296–1323.
[21] J.E. Anthony, Functionalized acenes and heteroacenes for organic electronics, Chemical Reviews 106 (2006) 5028–5048.
[22] M. Hissler, P.W. Dyer, R. Re'au, Linear organic π-conjugated systems featuring the heavy group 14 and 15 elements, Coordination Chemistry Reviews 244 (2003) 1–44.
[23] S.H. Lee, D.J. Choo, S.H. Han, J.H. Kim, Y.R. Son, J. Jang, High performance organic thin-film transistors with photopatterned gate dielectric, Applied Physics Letters 90 (2007) 33502–33504.
[24] A. Hepp, H. Heil, W. Weise, M. Ahles, R. Schmechel, H. von Seggern, Light-emitting field-effect transistor based on a tetracene thin film, Physical Review Letters 91 (2003) 157406–157409.
[25] M. Muccini, A bright future for organic field-effect transistors, Nature Materials 5 (2006) 605–613.
[26] B.B.Y. Hsu, C. Duan, E.B. Namdas, A. Gutacker, J.D. Yuen, F. Huang, Y. Cao, G.C. Bazan, I.D.W. Samuel, A.J. Heeger, Control of efficiency, brightness, and recombination zone in light-emitting field effect transistors, Advanced Materials 24 (2012) 1171–1175.
[27] H.-S. Seo, D.-K. Kim, J.-D. Oh, E.-S. Shin, J.-H. Choi, Organic light-emitting field-effect transistors based upon pentacene and perylene, Journal of Physical Chemistry C 117 (2013) 4764–4770.
[28] S. Dufresne, G.S. Hanan, W.G. Skene, Preparation, photophysics, and electrochemistry of segmented comonomers consisting of thiophene and pyrimidine units: new monomers for hybrid copolymers, Journal of Physical Chemistry B 111 (2007) 11407–11418.
[29] V. Coropceanu, J. Cornil, D.A. da Silva Filho, Y. Olivier, R. Silbey, J.-L. Bre'das, Charge transport in organic semiconductors, Chemical Reviews 107 (2007) 926–952.
[30] (a) R.S. Sanchez-Carrera, V. Coropceanu, D.A. da Silva, R. Friedlein, W. Osikowicz, R. Murdey, C. Suess, W.R. Salaneck, J.L. Bredas, Vibronic coupling in the ground and excited states of oligoacene cations, Journal of Physical Chemistry B 110 (2006) 18904–18911;
(b) N.E. Gruhn, D.A. da Silva Filho, T.G. Bill, M. Malagoli, V. Coropceanu, A. Kahn, J.-L. Bre'das, The vibrational reorganization energy in pentacene: molecular influences on charge transport, Journal of the American Chemical Society 124 (2002) 7918–7919.
[31] (a) A. Irfan, A.G. Al-Sehemi, DFT study of the electronic and charge transfer properties of perfluoroarene–thiophene oligomers, Journal of Saudi Chemical Society (2011), http://dx.doi.org/10.1016/j.jscs.2011.11.006;
(b) A. Irfan, H. Aftab, A.G. Al-Sehemi, Push–pull effect on the geometries, electronic and optical properties of thiophene based dye-sensitized solar cell materials, Journal of Saudi Chemical Society (2011), http://dx.doi.org/10.1016/j.jscs.2011.11.013;
(c) A. Irfan, A.G. Al-Sehemi, Energy decomposition analysis of "H/OH" derivatives of the meridianal isomer of tris(8-hydroxyquinoli nato)aluminum (*mer*-Alq3), Journal of the Chemical Society of Pakistan 34 (2012) 350–354;
(d) A. Irfan, A.G. Al-Sehemi, A.M. Asiri, M. Nadeem, K.A. Alamry, A study on the electronic and charge transfer properties in tin phthalocyanines (SnPc) derivatives by density functional theory, Computational and Theoretical Chemistry 977 (2011) 9–12;
(e) A. Irfan, A.G. Al-Sehemi, S. Muhammad, J. Zhang, Packing effect on the transfer integrals and mobility in 9-bis(dithieno[3,2-b:2,3-d]thiophene) (BDT) and its heteroatom-substituted analogues, Australian Journal of Chemistry 64 (2011) 1587–1592;
(f) A.G. Al-Sehemi, A. Irfan, A.M. Asiri, Y.A. Ammar, Synthesis, characterization and DFT study of methoxybenzylidene containing chromophores for DSSC, Spectrochimica Acta Part A: Molecular and Biomolecular 91 (2012) 239–243;
(g) A.G. Al-Sehemi, A. Irfan, A.M. Asiri, Y.A. Ammar, Molecular design of new hydrazone dyes for dye-sensitized solar cells: synthesis, characterization and DFT study, Journal of Molecular Structure 1019 (2012) 130–134;
(h) A. Irfan, N. Hina, A.G. Al-Sehemi, A.M. Asiri, Quantum chemical investigations towards modeling of highly efficient zinc porphyrin dye sensitized solar cells, The Journal of Molecular Modeling 18 (2012) 4199–4207;

(i) A.G. Al-Sehemi, A. Irfan, A.M. Asiri, The DFT investigations of the electron injection in hydrazone-based sensitizers, Theoretical Chemistry Accounts 131 (2012) 1199–1208;
(j) A. Irfan, A.G. Al-Sehemi, Quantum chemical study in the direction to design efficient donor-bridge-acceptor triphenylamine sensitizers with improved electron injection, The Journal of Molecular Modeling 18 (2012) 4893–4900;
(k) A. Irfan, R. Jin, A.G. Al-Sehemi, A.M. Asiri, Quantum chemical study of the donor-bridge-acceptor triphenylamine based sensitizers, Spectrochimica Acta Part A: Molecular and Biomolecular Spectroscopy (2013), http://dx.doi.org/10.1016/j.saa.2013.02.045.

[32] A.D. Becke, Density-functional thermochemistry. III. The role of exact exchange, Journal of Chemical Physics 98 (1993) 5648–5652.

[33] B. Miehlich, A. Savin, H. Stoll, H. Preuss, Results obtained with the correlation energy density functionals of becke and Lee, Yang and Parr, Chemical Physics Letters 157 (1989) 200–206.

[34] C. Lee, W. Yang, R.G. Parr, Development of the Colle–Salvetti correlation-energy formula into a functional of the electron density, Physical Review B 37 (1988) 785–789.

[35] (a) G.A. Petersson, A. Bennett, T.G. Tensfeldt, M.A. Al-Laham, W.A. Shirley, J. Mantzaris, A complete basis set model chemistry. I. The total energies of closed-shell atoms and hydrides of the first-row atoms, Journal of Chemical Physics 89 (1988) 2193–2218;
(b) G.A. Petersson, M.A. Al-Laham, A complete basis set model chemistry. II. Open-shell systems and the total energies of the first-row atoms, Journal of Chemical Physics 94 (1991) 6081–6090.

[36] C.R. Zhang, W.Z. Liang, H.S. Chen, Y.H. Chen, Z.Q. Wei, Y.Z. Wu, Theoretical studies on the geometrical and electronic structures of N-methyle-3,4-fulleropyrrolidine, Journal of Molecular Structure (Theochem) 862 (2008) 98–104.

[37] D. Matthews, P. Infelta, M. Grätzel, Calculation of the photocurrent-potential characteristic for regenerative, sensitized semiconductor electrodes, Solar Energy Materials and Solar Cells 44 (1996) 119–155.

[38] R. Bauernschmitt, R. Ahlrichs, Treatment of electronic excitations within the adiabatic approximation of time dependent density functional theory, Chemical Physics Letters 256 (1996) 454–464.

[39] M.E. Casida, C. Jamorski, K.C. Casida, D.R. Salahub, Molecular excitation energies to high-lying bound states from time-dependent density-functional response theory: characterization and correction of the time-dependent local density approximation ionization threshold, Journal of Chemical Physics 108 (1998) 4439–4449.

[40] R.E. Stratmann, G.E. Scuseria, M.J. Frisch, An efficient implementation of time-dependent density-functional theory for the calculation of excitation energies of large molecules, Journal of Chemical Physics 109 (1998) 8218–8224.

[41] C. Van Caillie, R.D. Amos, Geometric derivatives of excitation energies using SCF and DFT, Chemical Physics Letters 308 (1999) 249–255.

[42] C. Van Caillie, R.D. Amos, Geometric derivatives of density functional theory excitation energies using gradient-corrected functionals, Chemical Physics Letters 317 (2000) 159–164.

[43] F. Furche, R. Ahlrichs, Adiabatic time-dependent density functional methods for excited state properties, Journal of Chemical Physics 117 (2002) 7433–7447.

[44] G. Scalmani, M.J. Frisch, B. Mennucci, J. Tomasi, R. Cammi, V. Barone, Geometries and properties of excited states in the gas phase and in solution: theory and application of a time-dependent density functional theory polarizable continuum model, Journal of Chemical Physics 124 (2006) 094107.

[45] A. Irfan, R. Cui, J. Zhang, L. Hao, Push–pull effect on the charge transfer, and tuning of emitting color for disubstituted derivatives of *mer*-Alq3, Chemical Physics 364 (2009) 39–45.

[46] N.C. Greenham, S.C. Moratti, D.D.C. Bradley, R.H. Friend, A.B. Holmes, Efficient light-emitting diodes based on polymers with high electron affinities, Nature (London) 365 (1993) 628–630.

[47] R.A. Marcus, N. Sutin, Electron transfers in chemistry and biology, Biochimica et Biophysica Acta 811 (1985) 265–322.

[48] E.V. Tsiper, Z.G. Soos, W. Gao, A. Kahn, Electronic polarization at surfaces and thin films of organic molecular crystals: PTCDA, Chemical Physics Letters 360 (2002) 47–52.

[49] J.L. Bredas, J.P. Calbert, D.A. da Silva Filho, J. Cornil, Organic semiconductors: a theoretical characterization of the basic parameters governing charge transport, Proceedings of the National Academy of Sciences 99 (2002) 5804–5809.

[50] B.C. Lin, C.P. Cheng, Z.Q. You, C.P. Hsu, Charge transport properties of tris(8-hydroxyquinolinato)aluminum(III): why it is an electron transporter, Journal of the American Chemical Society 127 (2005) 66–67.

[51] Z.G. Soos, E.V. Tsiper, A. Painelli, Polarization in organic molecular crystals and charge-transfer salts, Journal of Luminescence 110 (2004) 332–341.

[52] E.V. Tsiper, Z.G. Soos, Electronic polarization in pentacene crystals and thin films, Physical Review B 68 (2003) 085301–085310.

[53] M.J. Frisch, G.W. Trucks, H.B. Schlegel, G.E. Scuseria, M.A. Robb, J.R. Cheeseman, G. Scalmani, V. Barone, B. Mennucci, G.A. Petersson, H. Nakatsuji, M. Caricato, X. Li, H.P. Hratchian, A.F. Izmaylov, J. Bloino, G. Zheng, J.L. Sonnenberg, M. Hada, M. Ehara, K. Toyota, R. Fukuda, J. Hasegawa, M. Ishida, T. Nakajima, Y. Honda, O. Kitao, H. Nakai, T. Vreven, J.A. Montgomery Jr., J.E. Peralta, F. Ogliaro, M. Bearpark, J.J. Heyd, E. Brothers, K.N. Kudin, V.N. Staroverov, R. Kobayashi, J. Normand, K. Raghavachari, A. Rendell, J.C. Burant, S.S. Iyengar, J. Tomasi, M. Cossi, N. Rega, J.M. Millam, M. Klene, J.E. Knox, J.B. Cross, V. Bakken, C. Adamo, J. Jaramillo, R. Gomperts, R.E. Stratmann, O. Yazyev, A.J. Austin, R. Cammi, C. Pomelli, J.W. Ochterski, R.L. Martin, K. Morokuma, V.G. Zakrzewski, G.A. Voth, P. Salvador, J.J. Dannenberg, S. Dapprich, A.D. Daniels, Ö. Farkas, J.B. Foresman, J.V. Ortiz, J. Cioslowski, D.J. Fox, Gaussian 09, Revision A. 1, Gaussian, Inc., Wallingford, CT, 2009.

[54] T. Stein, L. Kronik, R. Baer, Prediction of charge-transfer excitations in coumarin-based dyes using a range-separated functional tuned from first principles, Journal of Chemical Physics 131 (2009) 244119–244123.

[55] B.M. Wong, M. Piacenza, F.D. Sala, Absorption and fluorescence properties of oligothiophene biomarkers from long-range-corrected time-dependent density functional theory, Physical Chemistry Chemical Physics 11 (2009) 4498–4508.

[56] B.M. Wong, J.G. Cordaro, Coumarin dyes for dye-sensitized solar cells: a long-range-corrected density functional study, Journal of Chemical Physics 129 (2008) 214703–214710.

[57] A.W. Lange, M.A. Rohrdanz, J.M. Herbert, Charge-transfer excited states in a $\pi$-stacked adenine dimer, as predicted using long-range-corrected time-dependent density functional theory, The Journal of Physical Chemistry B 112 (2008) 6304–6308.

[58] M.A. Rohrdanz, J.M. Herbert, Simultaneous benchmarking of ground- and excited-state properties with long-range-corrected density functional theory, Journal of Chemical Physics 129 (2008) 034107–034115.

[59] J. Toulouse, F. Colonna, A. Savin, Short-range exchange and correlation energy density functionals: beyond the local-density approximation, Journal of Chemical Physics 122 (2005) 014110–014119.

[60] E. Livshits, R. Baer, A well-tempered density functional theory of electrons in molecules, Physical Chemistry Chemical Physics 9 (2007) 2932–2941.

[61] W. Xu, B. Peng, J. Chen, M. Liang, F. Cai, New triphenylamine-based dyes for dye-sensitized solar cells, The Journal of Physical Chemistry C 112 (2008) 874–880.

[62] J. Preat, D. Jacquemi, E.A. Perpete, Design of new triphenylamine-sensitized solar cells: a theoretical approach, Environmental Science & Technology 44 (2010) 5666–5671.

[63] J. Preat, C. Michaux, D. Jacquemin, E.A. Perpe'te, Enhanced efficiency of organic dye-sensitized solar cells: triphenylamine derivatives, The Journal of Physical Chemistry C 113 (2009) 16821–16833.

[64] A.D. Becke, A new mixing of Hartree–Fock and local density-functional theories, Journal of Chemical Physics 98 (1993) 1372–1377.

[65] A.D. Becke, Density-functional exchange-energy approximation with correct asymptotic behavior, Physical Review A 38 (1988) 3098–3100.

[66] R. Krishnan, J.S. Binkley, R. Seeger, J.A. Pople, Self-consistent molecular orbital methods. XX. A basis set for correlated wave functions, Journal of Chemical Physics 72 (1980) 650–655.

[67] R.K. Chan, S.C. Liao, Dipole moments, charge-transfer parameters, and ionization potentials of the methyl-substituted benzene–tetracyanoethylene complexes, Canadian Journal of Chemistry 48 (1970) 299–305.